Computational Materials Science 112 (2016) 269–275

Contents lists available at ScienceDirect

Computational Materials Science

journal homepage: www.elsevier.com/locate/commatsci

Study of interaction between transition metal atoms and bigraphene monovacancy by means of quantum chemistry

Alexander A. Kuzubov [a,b], Pavel V. Avramov [c], Kristina M. Nikolaeva [a], Natalya S. Mikhaleva [a], Evgenia A. Kovaleva [a,*], Artem V. Kuklin [a], Alexander S. Fedorov [b]

[a] Siberian Federal University, 79 Svobodny pr., Krasnoyarsk 660041, Russia
[b] L.V. Kirensky Institute of Physics, 50 Akademgorodok, Krasnoyarsk 660036, Russia
[c] Kyungpook National University, 80 Daehakro, Bukgu, Daegu 41566, Republic of Korea

ARTICLE INFO

Article history:
Received 26 August 2015
Received in revised form 30 October 2015
Accepted 2 November 2015
Available online 19 November 2015

Keywords:
Bigraphene
Spintronics
Transition metal
Adsorption
Migration

ABSTRACT

First-row transition metal atoms adsorption on bigraphene monovacancy was studied within the framework of DFT in periodic boundary conditions. Electronic and magnetic properties of composites were analyzed and their potential utilization in spintronics was discussed. Barriers of metal atoms migration from bigraphene surface to the interlayer space through the vacancy were estimated in order to consider both thermodynamic and kinetic aspects of composites experimental preparation. Formation of metal atoms inner-sorbed on bigraphene was found to demand harsh synthesis conditions; whereas outer-sorbed composites demonstrate significantly higher degree of spin polarization which makes them perspective for usage in spintronic devices.

1. Introduction

A large number of theoretical and experimental studies are concerned with graphene and its electronic properties [1,2]. This material is of a great interest due to its unique properties provided by the presence of Dirac cones [3–5].

Electronic and magnetic structure of graphene can be changed significantly by its doping. This effect is also known as Kondo effect and may be implemented in spintronics [6–9]. Rather big transition metal atoms can be adsorbed on the graphene as adatoms and replace one or two carbon atoms [10–12].

The knowledge about the interaction between transition metal and sp^2 carbon atom is essential for understanding carbon nanotubes growing mechanism [13], fuel cell properties [14], and possibility of magnetic ordering in carbon-based materials by doping with magnetic metals, for instance, Fe [15].

Sorption of transition metals, namely, 3d-metals (Sc–Zn), Au, Pt, was investigated experimentally [11,16] and theoretically [10–12,17–20]. All metals were found to prefer the adsorption on graphene vacancies. Strong covalent bonding between transition metal atom and carbon 2D structure makes these structures more stable than others.

Binding energy of transition metal with mono- or bivacancy lies in the range of 2–8 eV [10,17–20]. In contrast with Cu, Zn, Pt and Au, metals from Sc to Ni are likely to adsorb rather on bivacancy than monovacancy [10].

All the abovementioned structures [10] may be divided into four groups according to their magnetic properties: both mono- and bivacancy are non-magnetic (Sc, Ti, Ni, Zn, Pt); monovacancy is magnetic (μ_{Cu} = 1.5 μ_B, μ_{Au} = 1 μ_B) while bivacancy is not; opposite case of non-magnetic monovacancy and magnetic bivacancy (μ_{Fe} = 3.2 μ_B); both mono- (μ_V = 1 μ_B, μ_{Cr} = 2 μ_B, μ_{Mn} = 3 μ_B, μ_{Co} = 1 μ_B) and bivacancy (μ_V = 3 μ_B, μ_{Cr} = 2 μ_B, μ_{Mn} = 3 μ_B, μ_{Co} = 1.5 μ_B) are magnetic.

Composites containing Fe, Mn, V show much bigger values of magnetic moment and, hence, are the most interesting for spintronics applications. Low mobility of vacancies along with adsorbed TM atoms is one more advantage of these materials due to the high migration barriers [10,16,20].

Method proposed [10] for experimental preparation of described composites involves irradiation by the focused electron beam in order to reach the atomic precision of defect creation which is followed by the high temperature coprecipitation of metal atoms.

This method was implemented for Fe, Co, Mo, Pt and In atoms [21,22]. All methods of defect creation and doping of graphene with a precise spatial control are quite difficult and have some

* Corresponding author. Tel.: +7 (923)2764752; fax: +7 (391)2062109.
E-mail address: kovaleva.evgeniya1991@mail.ru (E.A. Kovaleva).

http://dx.doi.org/10.1016/j.commatsci.2015.11.002
0927-0256/

constraints, but they are very important in graphene properties control.

Recent studies showed that vacancies in graphene may be created with a spatial precision of $10 \times 10\ nm^2$ by the electron beam irradiation with accelerating voltage of 80 kV [23,24]. Enhanced chemical activity of these vacancies gives a possibility of the surface adatom capture.

Similar studies were also performed for bigraphene containing a monovacancy and adsorbed metal atom (Au, Mn, Mo) [25–27]. Doping of bigraphene epitaxially grown on 4H–SiC (0001) by Mo was investigated by both experimental and theoretical techniques. Molybdenum atoms were found to replace α-carbon atoms and occupy the interlayer space [25]. Local magnetic moment of Mo atom is equal to 1.81 μ_B in this case. Composites of Mn and Au atoms adsorbed on the monovacancy and carbon atom in bigraphene have been simulated [26,27]. Charge transfer of 1.6 e to the defect-free graphene layer was observed in the case of Au doping. Local magnetic moment of Mn (1.76 μ_B) and high spin polarization of composite suggests the possibility of electron separation by the spin.

The present study is aimed to reveal the features of transition metals sorption on the bigraphene monovacancy by means of quantum chemistry. Metal atom migration from surface to the interlayer space through the monovacancy is also discussed.

2. Computational methods

Quantum chemical modeling was performed by generalized gradient approximation (GGA) of density functional theory (DFT) [28,29], plane wave basis set and PAW formalism [30,31] using VASP code [32–34]. Perdew–Burke–Ernzerhof (PBE) exchange–correlation functional with the dispersion correction of Grimme [35] was used for taking into account van der Waals interactions.

Transition state and energy barriers of transition metal atom migration from the surface to the interlayer space through the monovacancy were found by using nudged elastic band (NEB) method [36].

Hexagonal unit cell of bigraphene ($a = b = 2.45$ Å, $c = 3.33$ Å) was optimized as a first step. Then, bigraphene supercell containing $5 \times 5 \times 1$ unit cells and a single monovacancy was simulated. Two different positions of vacancy were considered (Fig. 1): the first is placed directly above the carbon atom in adjacent layer (*top*), and the second one is on top of the middle of the hexagon (*hex*).

The Monkhorst–Pack [37] *k*-point Brillioin sampling was used during the optimization. The *k*-point grid contained $12 \times 12 \times 1$ points in the case of unit cell, and $3 \times 3 \times 1$ points for supercell, respectively.

To avoid artificial interactions between adjacent bigraphene images in periodic boundary conditions, a vacuum interval along the normal direction to the carbon planes was fixed as 20 Å. Energy cutoff was specified as 400 eV. Maximum acting forces being equal to 0.01 eV/ Å were used as a stopping criterion for geometry optimization.

3. Results and discussion

3.1. Stability and properties of TM/bigraphene composites

The *top* vacancy was found to be more energetically favorable than the *hex* one. Formation energy of this vacancy is equal to 7.70 eV and its magnetic moment is 1.2 μ_B, while the formation energy of *hex* monovacancy is equal to 7.81 eV, and corresponding magnetic moment is 0.9 μ_B.

Probabilities of vacancy formation were estimated according to the Gibbs distribution:

$$P_i = \frac{e^{-\frac{E_{V_i}}{k_B T}}}{\sum_{i=1}^{2} e^{-\frac{E_{V_i}}{k_B T}}}, \quad (1)$$

where E_{V_i} is the formation energy of *top* or *hex* vacancy, correspondingly.

Low mobility of monovacancies in graphene at normal conditions (migration barrier is equal to ~1.17 eV [38]) allows to suppose that bigraphene vacancies will be formed according to their thermodynamic stability (see Table 1). It can be clearly seen that *top* vacancy is dominating in wide temperature range. However, formation of *hex* structure still may occur when TM atoms are deposited on bigraphene. Keeping this in mind, we then considered both types of composites.

Sorption of 3d transition metals, namely, Cr, Fe, Mn, Ti and V, was studied for structures with transition metal atoms adsorbed on the bigraphene surface (hereafter TM_{out}), and also for those intercalated into the interlayer space (hereafter TM_{in}) Transition metal atoms were adsorbed on monovacancy in both cases. For the sake of comparison binding energy of metal atoms with bigraphene was calculated as:

$$E = E_{total} - E_{defect} - E_{Me}/n, \quad (2)$$

where E_{total} is total energy of hybrid system, E_{defect} is energy of bigraphene supercell containing monovacancy, E_{Me} is unit cell energy of corresponding metal, and n is number of metal atoms in unit cell (for the most stable modification).

For better understanding of binding features, total energies of hybrid structure were also reduced to the most stable one for each type of metal.

According to our results (see Table 2), all metals tend to locate in the interlayer space which can be attributed to higher degree of coordinational saturation in this case comparing with adsorption on the surface.

Formation of additional bonds with carbon atoms leads to increase of TM atom positive charge. This, in turn, results in higher

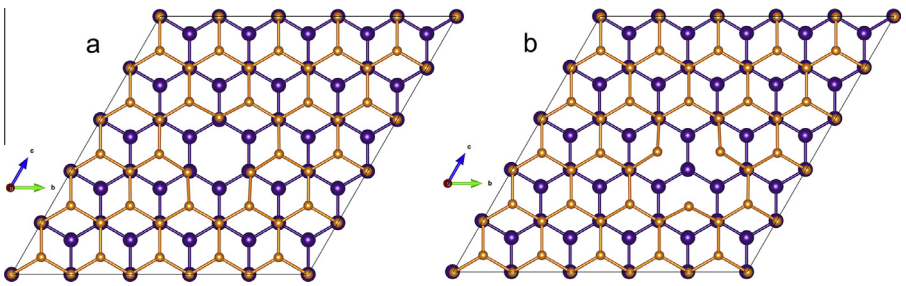

Fig. 1. (a) *hex* and (b) *top* type of bigraphene monovacancy. First- and second-layer carbon atoms are denoted as orange and purple balls, correspondingly. (For interpretation of the references to color in this figure legend, the reader is referred to the web version of this article.)

Table 1
Thermodynamic probabilities of formation of *top* (P1) and *hex* (P2) type of monovacancy.

T, K	298	398	498	600	700	800	900	1000	1100	1200	1300
P1, %	98.6	96.1	92.9	89.4	86.1	83.1	80.5	78.2	76.1	74.3	72.8
P2, %	1.4	3.9	7.3	10.6	13.9	16.9	19.5	21.8	23.9	25.7	27.3

Table 2
Values of binding energies including ones reduced to the most stable configuration depending on type of metal, type of vacancy and type of sorption.

Type of Me	Inner sorption		Outer sorption	
	hex	*top*	*hex*	*top*
Binding energy, eV				
Ti	−3.25	−2.89	−2.61	−2.60
V	−2.76	−2.39	−1.87	−1.86
Cr	−2.79	−2.45	−1.93	−1.91
Mn	−2.93	−2.73	−2.18	−2.16
Fe	−3.21	−2.98	−2.31	−2.28
Binding energy reduced to the most stable configuration, eV				
Ti	0	0.244	0.638	0.535
V	0	0.253	0.890	0.780
Cr	0	0.224	0.853	0.763
Mn	0	0.085	0.743	0.649
Fe	0	0.117	0.902	0.817

polarization and, hence, increases binding energy (see Table 3). It's worthnoting that complexes of TM atoms with *hex*-type structure are more favorable than *top* ones when TM is located in the interlayer space.

In contrast to that, *top* configuration is more stable for metal adsorption on the outer surface of bigraphene (see Table 3). Here, higher stability of this structure is due to the polarization of the second bigraphene layer.

Positive charge of TM atom adsorbed on *top* vacancy induces negative charge on the next-layer carbon atom (Table 3). Electrostatic interaction stabilizes TM positive charge and increases stability of *top* structure (see Fig. 2).

Magnetic moments for all considered structure are summarized in Table 3. Composites of Cr, Mn and V with bigraphene were found to be interesting for potential applications in spintronics due to the presence of magnetic moment. It should be pointed out that magnetic moment maintains regardless to the type of vacancy and metal location (TM_{in} and TM_{out}). Values of magnetic moments are in agreement with previous data regarding graphene monolayer [10].

Composites with TM atom adsorbed on the outer surface of bigraphene are 100% spin-polarized at the Fermi level. In contrast

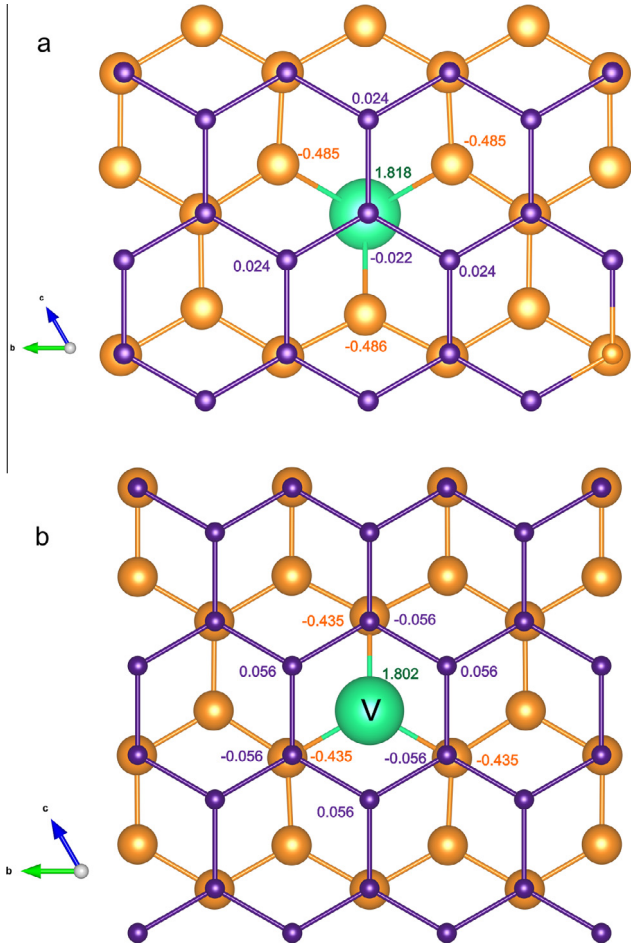

Fig. 2. Charges on vanadium and carbon atoms. Each value is denoted by the same color as the atom. Orange and purple balls correspond to the first and second-layer carbon atoms, respectively. (For interpretation of the references to color in this figure legend, the reader is referred to the web version of this article.)

Table 3
Values of total magnetic moment and charge on TM atom depending on type of metal, type of vacancy and type of sorption.

Type of Me	Inner sorption		Outer sorption	
	hex	*top*	*hex*	*top*
Magnetic moment, μ_B				
Ti	0.00	0.00	0.00	0.00
V	0.94	0.95	1.00	1.00
Cr	2.00	2.00	2.00	2.00
Mn	1.87	2.32	3.00	3.00
Fe	0.00	0.00	0.00	0.00
Charge, e				
Ti	2.3719	2.3358	2.1770	2.2314
V	1.9448	1.9372	1.8020	1.8184
Cr	1.6004	1.5660	1.4017	1.4839
Mn	1.4272	1.4158	1.2611	1.2721
Fe	1.0770	1.0637	1.0298	1.0337

to that, only Mn/bigraphene composite possess substantial degree of spin polarization among all structures with inner-sorbed metal atoms. Other ones demonstrate either low polarization ($V_{in/top}$) or no polarization at all.

This can be explained in terms of unpaired electrons localized on non-bonding d-orbital of TM_{out} adsorbed atom. This orbital lies at the Fermi level (see Fig. 3) in the gap caused by the presence of defect in graphene atomic structure. Nevertheless, the PDOS analysis shows that peaks corresponding to Dirac cones in bigraphene still can be recognized, though being shifted and supplemented by peaks originating from the hybridized states of π-conjugated system with d-orbitals of TM atoms (Fig. 4).

Thus, these structures are magnetic semiconductors with different band gaps for spin-up and spin-down channel. The energy of non-bonding d-orbital is shifted down from the Fermi level when number of d-electrons increases (from V to Mn) which can be attributed to the higher overlap with carbon orbitals (see Fig. 3).

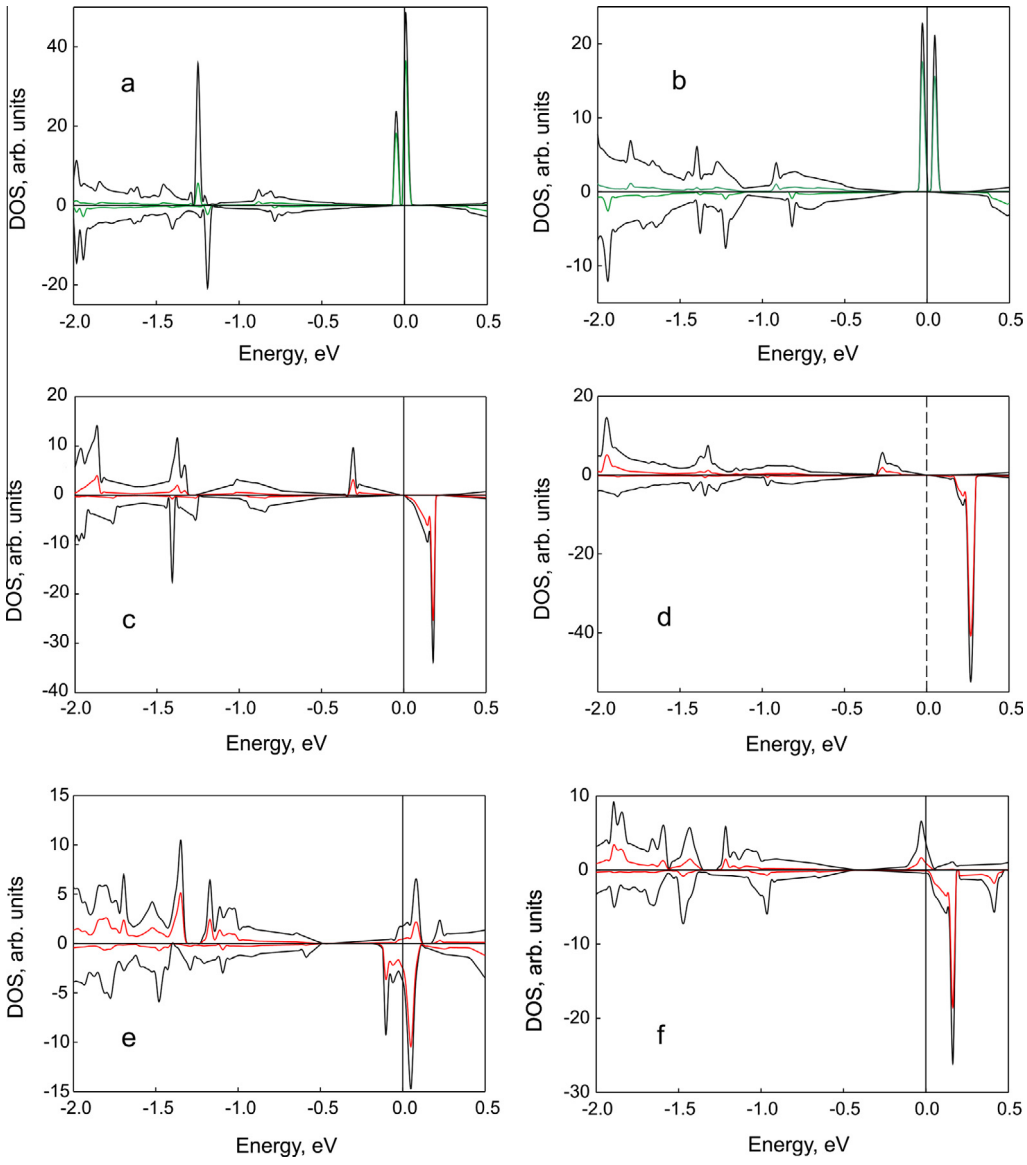

Fig. 3. Densities of states for (a) $V_{out/hex}$, (b) $V_{out/top}$, (c) $Mn_{out/hex}$, (d) $Mn_{out/top}$, (e) $Mn_{in/hex}$, and (f) $Mn_{in/top}$ composites. Total (TDOS) and partial (PDOS) densities of states for *V* (Mn) atoms are represented by black and green (red) lines. (For interpretation of the references to color in this figure legend, the reader is referred to the web version of this article.)

Increasing number of unpaired electrons also reduces band gap width and enhances spin polarization of opposite graphene layer (from 0.033 μ_B in $V_{out/top}$ to 0.263 μ_B in $Mn_{out/top}$). Spin density is distributed equally through the whole opposite graphene sheet (see Fig. 5).

Higher overlap of TM d-oribtals with carbon atom due to adsorption between graphene layers lead to their delocalization and decreases spin polarization of the system. Its value also depends on the type of the composite: since *hex* configuration promotes overlapping between TM and carbon orbitals more than *top* one, the degree of polarization and magnetic moment are lower in former case (see Fig. 3).

The analysis of DOS for Mn/bigraphene complexes is presented in Figs. 3 and 4.

As well as for outer-sorbed atoms, peaks corresponding to Dirac cones still present in electronic structure. They are, though, located significantly lower than Fermi level due to higher number of electrons in the system. Composites then possess metallic conductivity with different filling in major and minor spin at Fermi level. Maximal value of spin polarization corresponds to $Mn_{in/top}$.

3.2. Migration barriers between TM_{in} and TM_{out} composites

According to the binding energies, TM_{in} structures are substantially more favorable. In order to reveal possible kinetic drawbacks that may occur during the formation of these composites, we performed quantum chemical modeling of TM atom migration from the outer surface to the interlayer space and back through the vacancy.

Reaction paths and transition states were found by NEB method. Migration barriers are high in all cases (see Table 4) with minimum value equal to 2.55 eV for Fe adsorbed on *top* vacancy.

Potential barriers for TM metals change in agreement with their atomic radii. *Top* configurations show higher barriers of migration from the surface to the interlayer space than *hex* ones due to the higher binding energy between TM and bigraphene surface in former case. Difference between barriers is in agreement with difference in binding energy between TM_{top} and TM_{hex}.

Difference between direct and inverse reaction barriers indicates that migration constants are to be shifted to formation of

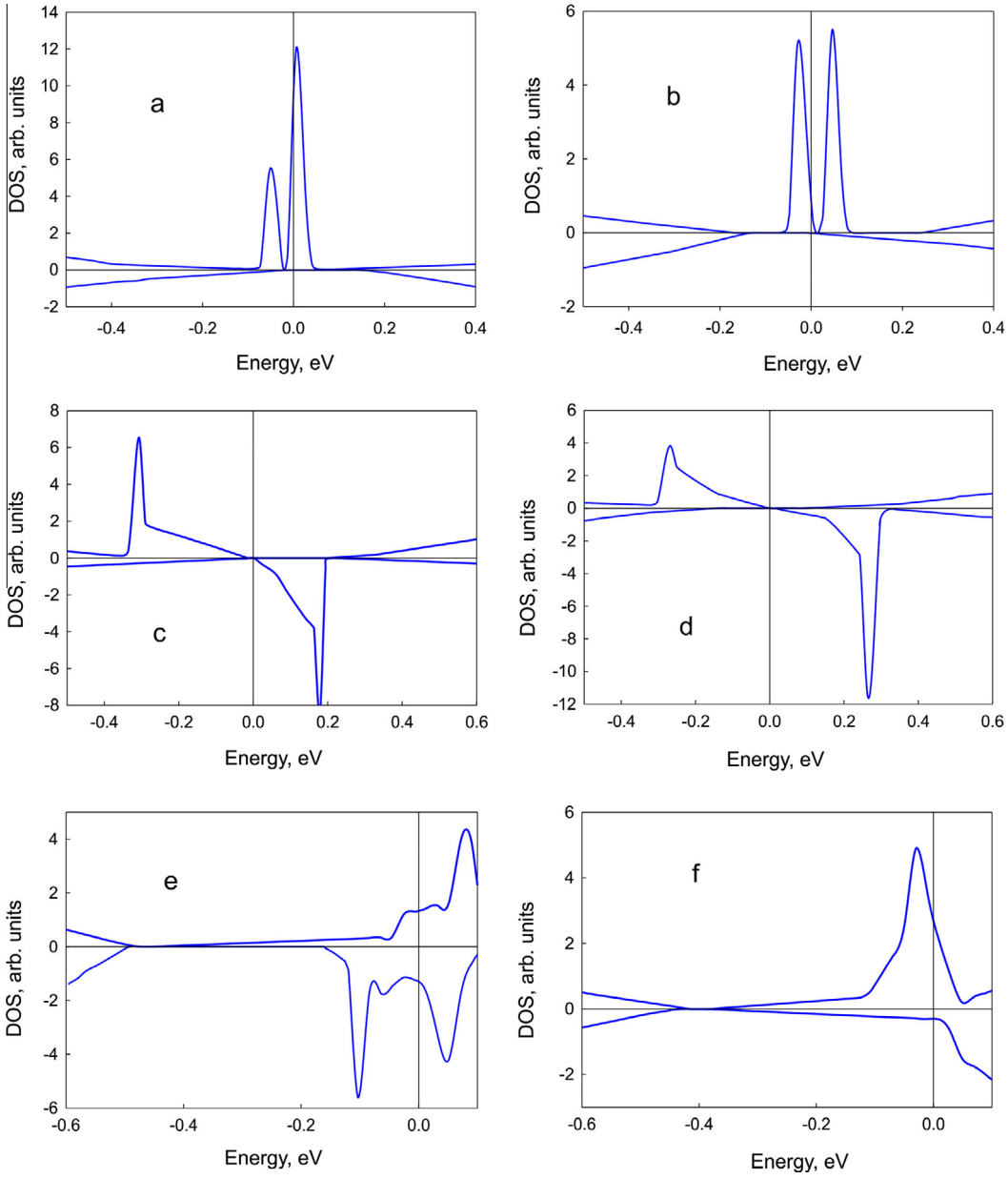

Fig. 4. Carbon PDOS for (a) $V_{out/hex}$, (b) $V_{out/top}$, (c) $Mn_{out/hex}$, (d) $Mn_{out/top}$, (e) $Mn_{in/hex}$, and (f) $Mn_{in/top}$ composites.

the inner-sorbed TM atom complexes. Nevertheless, high migration barrier may slow it down substantially.

Probability of Mn migration through *hex* vacancy versus temperature was evaluated using rate constants (see Table 5). This composite was chosen because of the high magnetic moment along with the relatively low migration barriers.

Rate constants were calculated using transition state theory:

$$k = Ae^{-\frac{E_{barrier}}{kT}}, \tag{3}$$

where A was estimated as [39]:

$$A = \frac{kT\prod_{i=1}^{3N-3}\left(1-e^{-\frac{h\nu_i}{kT}}\right)}{h\prod_{i=1}^{3N-4}\left(1-e^{-\frac{h\nu_i^{\#}}{kT}}\right)} \tag{4}$$

T is temperature, $E_{barrier}$ is the potential barrier height calculated as the energy difference between transition state and initial composite, product $\prod_{i=1}^{3N-3}\left(1-e^{-\frac{h\nu_i}{kT}}\right)$ corresponds to the minimum energy points and product $\prod_{i=1}^{3N-4}\left(1-e^{-\frac{h\nu_i^{\#}}{kT}}\right)$ corresponds to the transition state, ν_i is the frequency.

Zero-point energy was also taken into account when calculating potential barrier of migration by adding

$$E_i^{\#} = \sum_{i=1}^{3N-4}\frac{\hbar\nu_i^{\#}}{2} \tag{5}$$

to transition state energy and

$$E_0 = \sum_{i=1}^{3N-3}\frac{\hbar\nu_i}{2} \tag{6}$$

to the energy of initial structure. N is the number of atoms in system.

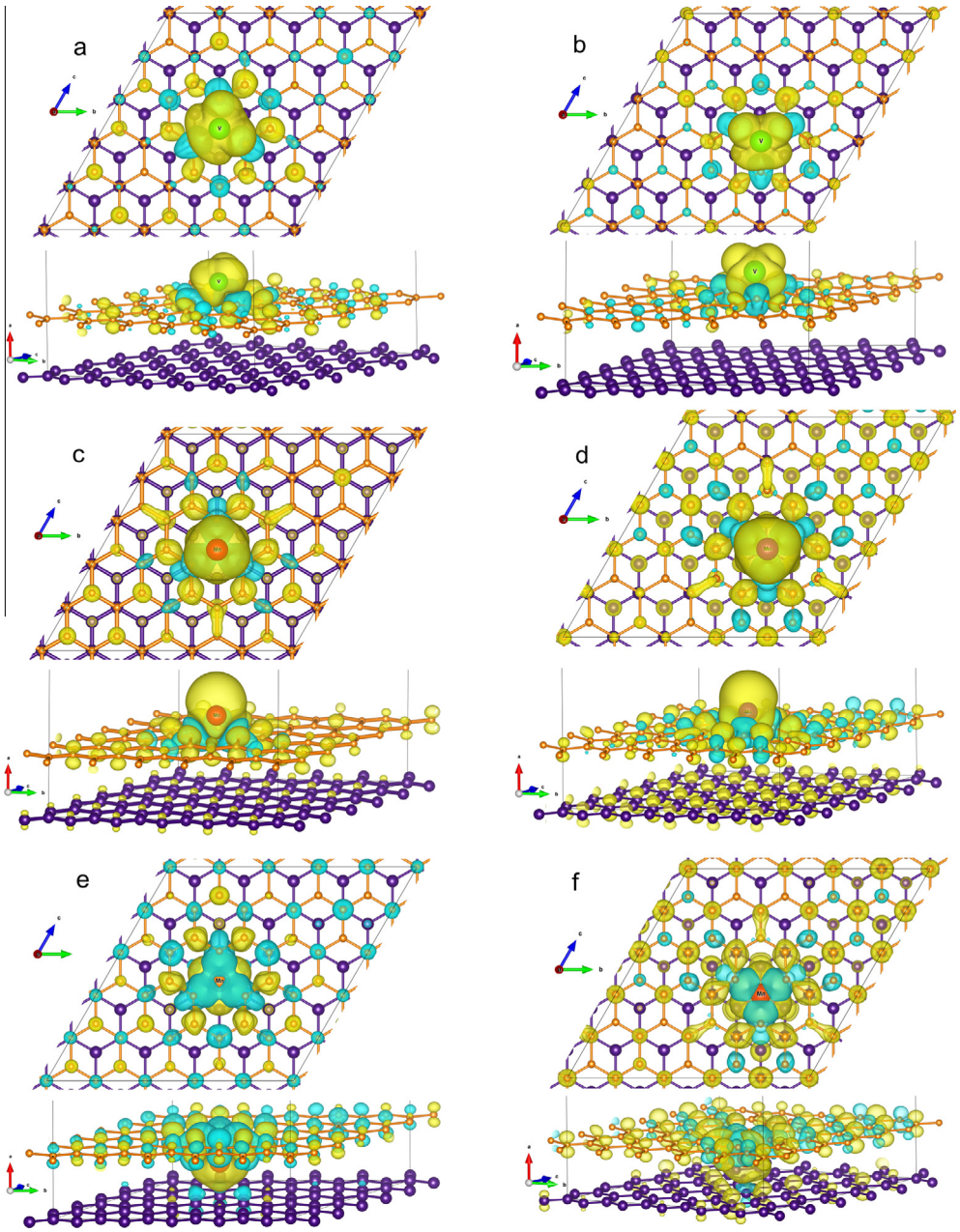

Fig. 5. Spatial distribution of spin density in (a) $V_{out/hex}$, (b) $V_{out/top}$, (c) $Mn_{out/hex}$, (d) $Mn_{out/top}$, (e) $Mn_{in/hex}$, and (f) $Mn_{in/top}$ composites. Yellow (blue) areas correspond to spin-up and spin-down density. (For interpretation of the references to color in this figure legend, the reader is referred to the web version of this article.)

Table 4
Migration barriers of TM jump from the bigraphene surface to the interlayer space through the vacancy.

Vacancy type	Me	Migration barrier, eV		Energy difference between inverse and direct barriers, eV
		To the interlayer space (direct)	To the outer surface (inverse)	
hex	Ti	5.820	6.595	0.775
	V	4.269	5.292	1.023
	Cr	3.475	4.761	1.286
	Mn	2.940	3.778	0.838
	Fe	2.553	3.601	1.048
top	Ti	5.942	6.234	0.292
	V	4.544	5.071	0.527
	Cr	3.441	4.547	1.106
	Mn	2.679	3.701	1.022
	Fe	2.180	3.608	1.428

Table 5
Values of pre-exponential Arrhenius factors (A), rate constants (k) and equilibrium constants (K) for Mn migration from the surface to the interlayer space of bigraphene through the *hex* monovacancy and back.

T, K	Direct		Inverse		K, k_1/k_2
	A, s^{-1}	k, s^{-1}	A, s^{-1}	k, s^{-1}	
298	$5.10 \cdot 10^{11}$	$4.81 \cdot 10^{-41}$	$1.87 \cdot 10^{12}$	$4.64 \cdot 10^{-53}$	$1.04 \cdot 10^{12}$
398	$5.20 \cdot 10^{11}$	$5.78 \cdot 10^{-28}$	$2.08 \cdot 10^{12}$	$8.82 \cdot 10^{-37}$	$6.56 \cdot 10^{8}$
498	$5.19 \cdot 10^{11}$	$3.83 \cdot 10^{-20}$	$2.19 \cdot 10^{12}$	$4.80 \cdot 10^{-27}$	$7.98 \cdot 10^{6}$
600	$5.11 \cdot 10^{11}$	$7.40 \cdot 10^{-15}$	$2.23 \cdot 10^{12}$	$1.83 \cdot 10^{-20}$	$4.04 \cdot 10^{5}$
700	$5.01 \cdot 10^{11}$	$3.56 \cdot 10^{-11}$	$2.25 \cdot 10^{12}$	$7.06 \cdot 10^{-16}$	$5.05 \cdot 10^{4}$
800	$4.90 \cdot 10^{11}$	$2.05 \cdot 10^{-8}$	$2.24 \cdot 10^{12}$	$1.93 \cdot 10^{-12}$	$1.06 \cdot 10^{4}$
900	$4.80 \cdot 10^{11}$	$2.85 \cdot 10^{-6}$	$2.22 \cdot 10^{12}$	$9.04 \cdot 10^{-10}$	$3.15 \cdot 10^{3}$
1000	$4.70 \cdot 10^{11}$	$1.47 \cdot 10^{-4}$	$2.20 \cdot 10^{12}$	$1.23 \cdot 10^{-7}$	$1.20 \cdot 10^{3}$
1100	$4.61 \cdot 10^{11}$	0.0037	$2.18 \cdot 10^{12}$	$6.87 \cdot 10^{-6}$	$5.39 \cdot 10^{2}$
1200	$4.53 \cdot 10^{11}$	0.0545	$2.16 \cdot 10^{12}$	0.00020	$2.79 \cdot 10^{2}$
1300	$4.46 \cdot 10^{11}$	0.5284	$2.14 \cdot 10^{12}$	0.0033	$1.59 \cdot 10^{2}$

In addition to that, equilibrium constants was calculated as the ratio of corresponding rate constants:

$$K = \frac{k_{approach}}{k_{removal}} \tag{7}$$

Activation energy was estimated to be 3.08 and 3.82 eV for direct and inverse process (with zero-point energy taken into account). Practically, this means that there should be one jump from bigraphene surface to the interlayer in 4.5 min at 1100 K (according to Table 5). Since the values of rate constants are even lower below 1000 K, migration of Mn to the interlayer space is very unlikely.

Formation of complexes with inner-sorbed TM atom is then limited by high migration barriers. It only can be possible in harsh annealing conditions (temperatures higher than 1000 K and long time of annealing). Since migration barriers are even higher for most of other complexes, it's reasonable to suppose that formation of inner complexes is unlikely. This, however, could be changed by adsorbing it not on mono- but on bivacancy in bigraphene.

4. Conclusion

Composites of bigraphene with outer-sorbed Cr, Mn and *V* atoms are magnetic semiconductors with high degree of spin polarization which allows using them in spintronic devices. Higher probability of *top* vacancy formation along with a little difference in binding energies of bigraphene vacancy with metal allows suggesting that $TM_{out/top}$ composites would be obtained predominately. Some amount of $TM_{out/hex}$ structures does not make a difference since electronic and magnetic properties of configurations are virtually the same. Complexes with inner-sorbed TM atoms possess metallic conductivity while spin polarization is significantly lower in that case. However, even though the adsorption of TM in the interlayer space is more thermodynamically favorable, according to migration barriers and equilibrium constants, the formation of these structures demands harsh conditions of synthesis. Usage of bivacancy instead of monovacancy could possibly reduce migration barriers and has to be investigated.

Acknowledgments

The authors would like to thank Siberian Supercomputer Center (SSCC) of SB RAS, Novosibirsk; and L.V. Kirensky Institute of Physics of SB RAS, Krasnoyarsk, for providing the access to their supercomputers. This work was supported by the government contract of the Ministry of Education and Science of the Russian Federation to Siberian Federal University (Grant No. 16.1500.2014/K).

References

[1] A.K. Geim, K.S. Novoselov, Nat. Mater. 6 (2007) 183–191.
[2] A.H. Castro Neto, F. Guinea, N.M. Peres, K.S. Novoselov, A.K. Geim, Rev. Mod. Phys. 81 (2009) 109–162.
[3] K.S. Novoselov, A.K. Geim, S.V. Morozov, D. Jiang, M.I. Katsnelson, I.V. Grigorieva, S.V. Dubonos, A.A. Firsov, Nature 438 (2005) 197–200.
[4] M.I. Katsnelson, K.S. Novoselov, A.K. Geim, Nat. Phys. 2 (2006) 620–625.
[5] C. Park, Y.W. Son, M.L. Cohen, S.G. Louie, Nat. Phys. 4 (2008) 213–217.
[6] M. Hentschel, F. Guinea, Phys. Rev. B 76 (115407) (2007).
[7] K. Sengupta, G. Baskaran, Phys. Rev. B 77 (045417) (2008).
[8] B. Dora, P. Thalmeier, Phys. Rev. B 76 (115435) (2007).
[9] A.V. Shytov, M.I. Katsnelson, L.S. Levitov, Phys. Rev. Lett. 99 (236801) (2007).
[10] A.V. Krasheninnikov, P.O. Lehtinen, A.S. Foster, P. Pyykko, R.M. Nieminen, Phys. Rev. Lett. 102 (126807) (2009).
[11] O. Cretu, A.V. Krasheninnikov, J.A. Rodriguez-Manzo, L. Sun, R. Nieminen, F. Banhart, Phys. Rev. Lett. 105 (196102) (2010).
[12] W. Zhang, L. Sun, Z. Xu, A.V. Krasheninnikov, P. Huai, Z. Zhu, F. Banhart, Phys. Rev. B 81 (125425) (2010).
[13] O.V. Yazyev, A. Pasquarello, Phys. Rev. Lett. 100 (156102) (2008).
[14] G. Che, B.B. Lakshmi, E.R. Fisher, C.R. Martin, Nature 393 (1998) 346–349.
[15] R. Sielemann, Y. Kobayashi, Y. Yoshida, H.P. Gunnlaugsson, G. Weyer, Phys. Rev. Lett. 101 (137206) (2008).
[16] Y. Gan, L. Sun, F. Banhart, Small 4 (2008) 587–591.
[17] E.J.G. Santos, A. Ayuela, S.B. Fagan, J. Mendes Filho, D.L. Azevedo, A.G. Souza Filho, D. Sanchez-Portal, Phys. Rev. B 78 (195420) (2008).
[18] E.J.G. Santos, A. Ayuela, D. Sanchez-Portal, New J. Phys. 12 (053012) (2010).
[19] P.Y. Xie, G.L. Zhuang, Y.A. Lu, J.G. Wang, X.N. Li, Acta Phys. Chim. Sin. 28 (2) (2012) 331–337.
[20] S. Malola, H. Häkkinen, P. Koskinen, Appl. Phys. Lett. 94 (043106) (2009).
[21] J.A. Rodriguez-Manzo, O. Cretu, F. Banhart, ACS Nano 4 (6) (2010) 3422–3428.
[22] H. Wang, Q. Wang, Y. Cheng, K. Li, Y. Yao, Q. Zhang, C. Dong, P. Wang, U. Schwingenschlögl, W. Yang, X.X. Zhang, Nano Lett. 12 (2012) 141–144.
[23] A.W. Robertson, C.S. Allen, Y. Wu, K. He, J. Olivier, J. Neethling, A.I. Kirkland, J.H. Warner, Nat. Commun. 3 (1144) (2012).
[24] A.W. Robertson, B. Montanari, K. He, J. Kim, C.S. Allen, Y.A. Wu, J. Olivier, J. Neethling, N. Harrison, A.I. Kirkland, J.H. Warner, Nano Lett. 13 (2013) 1468–1475.
[25] W. Wan, H. Li, H. Huang, S.L. Wong, L. Lv, Y. Gao, A.T.S. Wee, ACS Nano 8 (1) (2014) 970–976.
[26] Y. Mao, J. Zhong, Nanotechnology 19 (205708) (2008).
[27] Y. Mao, G.M. Stocks, J. Zhong, New J. Phys. 12 (033046) (2010).
[28] P. Hohenberg, W. Kohn, Phys. Rev. 136 (1964) B864–B871.
[29] W. Kohn, L.J. Sham, Phys. Rev. 140 (1965) A1133–A1138.
[30] P.E. Blöchl, Phys. Rev. B 50 (1994) 17953–17979.
[31] G. Kresse, J. Joubert, Phys. Rev. B 59 (1999) 1758–1775.
[32] G. Kresse, J. Hafner, Phys. Rev. B 47 (1993) 558–561.
[33] G. Kresse, J. Hafner, Phys. Rev. B 49 (1994) 14251–14269.
[34] G. Kresse, J. Furthmüller, Phys. Rev. B 54 (1996) 11169–11186.
[35] S. Grimme, J. Comp. Chem. 27 (2006) 1787–1799.
[36] G. Henkelman, H. Jonsson, J. Chem. Phys. 113 (2000) 9978–9985.
[37] H.J. Monkhorst, J.D. Pack, Phys. Rev. B 13 (1976) 5188–5192.
[38] A.S. Fedorov, D.A. Fedorov, Z.I. Popov, Yu.E. Anan'eva, N.S. Eliseeva, A.A. Kuzubov, J. Exp. Theor. Phys. 112 (5) (2011) 820–824.
[39] G.H. Vineyard, J. Phys. Chem. Sol. 3 (1) (1957) 121–127.